Available online at www.sciencedirect.com
ScienceDirect
Nuclear Instruments and Methods in Physics Research A 570 (2007) 399–413
NUCLEAR INSTRUMENTS & METHODS IN PHYSICS RESEARCH Section A
www.elsevier.com/locate/nima

Accelerator test of an angle detecting inclined sensor (ADIS) prototype with beams of ^{48}Ca and fragments

J.J. Connell*[,1], C. Lopate[1], R.B. McKibben[1], A. Enman[2]

Space Science Center, University of New Hampshire, Durham, NH 03824, USA

Received 12 July 2006; received in revised form 13 October 2006; accepted 13 October 2006
Available online 10 November 2006

Abstract

The measurement of cosmic rays and Solar energetic particles in space is basic to our understanding of the Galaxy, the Sun, phenomena in the Heliosphere and what has come to be known broadly as "space weather". For these reasons, cosmic ray instruments are common on both scientific spacecraft and operational spacecraft such as weather satellites.

The resource constraints on spacecraft generally mean that instruments that measure cosmic rays and Solar energetic particles must have low mass (a few kg) and low power (a few W), be robust and reliable yet still highly capable. Such instruments must identify ionic species (at least by element, preferably by isotope) from protons through the iron group. The charge and mass resolution of heavy ion instruments in space depends upon determining ions' angles of incidence. The Angle Detecting Inclined Sensor (ADIS) system is a highly innovative and uniquely simple detector configuration used to determine the angle of incidence of heavy ions in space instruments. ADIS replaces complex position sensing detectors (PSDs) with a system of simple, reliable and robust Si detectors inclined at an angle to the instrument axis.

In August 2004, we tested ADIS prototypes with a ^{48}Ca beam at the National Superconducting Cyclotron Laboratory's (NSCL) Coupled Cyclotron Facility (CCF). Among the analyses performed on the data taken at the NSCL, we demonstrate that our prototype design with an ADIS system has a charge resolution of less than 0.25*e*. We also present a more generalized analytic derivation of instrument response and report on the corresponding analysis of Monte-Carlo modeling data.

PACS: 29.40.Gx; 95.55.Vj

Keywords: Cosmic ray instruments; Solar energetic particle instruments; Hodoscopes; Tracking instruments; Spacecraft instruments

1. Introduction

The measurement of cosmic rays and solar energetic particles in space is basic to our understanding of the Galaxy, the Sun, phenomena in the Heliosphere (that region of space dominated by the plasma and magnetic field of the Sun) and what has come to be known broadly as "space weather." The study of space radiation, particularly heavy ions, is a major area of basic research in both space physics and astrophysics. A complete discussion of this rich and extensive field of research is far beyond the scope of this paper, but an excellent review can be found in Simpson [1]. The astrophysical implications of cosmic rays, for example, relate to the fields and plasmas of the interstellar medium; the possibility of a Galactic wind, which would be driven by the cosmic rays; the confinement time of cosmic rays in the Galaxy, measured with radioactive secondaries such as ^{10}Be, ^{26}Al, ^{36}Cl and ^{54}Mn; and the nucleosynthetic history of the cosmic ray source and the Galaxy. The broad importance of space weather is a result of its negative impact on man-made systems. Among the radiation effects of space weather are the failure of satellites and spacecraft; the diversion of aircraft on polar routes; and the exposure of

*Corresponding author. Tel.: +1 603 862 5096; fax: +1 603 862 3584.
E-mail address: james.connell@unh.edu (J.J. Connell).
[1]Also at: Department of Physics.
[2]Also at: Department of Mechanical Engineering. Presently: BAE Systems, IEWS, Nashua, NH, USA.

0168-9002/$ - see front matter © 2006 Elsevier B.V. All rights reserved.
doi:10.1016/j.nima.2006.10.097

astronauts to radiation, even to lethal doses when beyond the protection of the Earth's magnetosphere. Heavy ions are a particular concern for electronics in space owing to their large Linear Energy Transfer (LET). Other general effects include disruption of communications and failures in terrestrial power grids leading to blackouts (e.g. the province of Quebec for 9+ hours on March 13, 1989). Space radiation plays a crucial role in space weather: first, as an important effect in itself; second, as a precursor that can warn of other impending effects; and third, as a probe of the underlying physics. As a result, cosmic ray instruments are common on both scientific and operational spacecraft.

Resource constrained spacecraft generally require instruments that measure cosmic rays and solar energetic particles to have low mass (a few kg) and low power (a few W), be robust and reliable yet still highly capable. Such instruments must identify ionic species (at least by element, preferably by isotope) from protons through the iron group. The charge and mass resolution of heavy ion instruments in space depends upon determining ions' angles of incidence since space radiation is effectively omni-directional. For example, the most common methods of identifying heavy ion species in space radiation use $\Delta E/\Delta x$ measurements. Since Δx depends upon the angle of incidence, corrections are required. The Angle Detecting Inclined Sensor (ADIS) system is a highly innovative and uniquely simple detector configuration used to determine the angle of incidence of heavy ions in space instruments. ADIS (Fig. 1) replaces complex position sensing detectors (PSDs) with a system of simple, reliable and robust detectors inclined at an angle to the instrument axis [2].

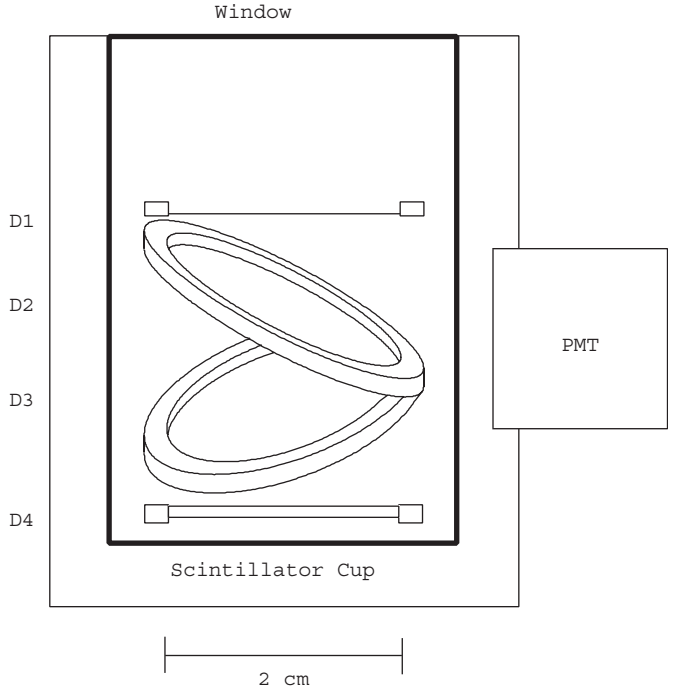

Fig. 1. Basic angle detecting inclined sensor configuration. D1, D2 and D3 are thin solid state detectors. D2 and D3 are inclined at 30° to the instrument axis, D2 with its major axis along the x-direction, and D3 along the y-direction. D4 serves as a stopping and residual energy detector. A scintillator cup viewed by a photomultiplier tube detects particles that penetrate D4, or exit the solid state detector stack. With a circular instrument aperture (defined by D1 and D4) D2 and D3 should be oval with the eccentricity determined by the angle of inclination.

As already noted, variations in the thickness of detector material particles traverse due to their different angles of incidence are the principal challenge in obtaining good charge and mass resolution in space based heavy ion telescopes. The ADIS takes advantage of this variation to determine the angle of incidence using a simple system of two detectors inclined to the telescope axis together with one detector normal to the axis. To demonstrate the ADIS concept in its most basic form, consider just the top two detectors. The normal to the inclined D2 is in the x–z plane. For a particle traveling in the x–z plane, let θ be the angle of incidence. The signal in D1 is then proportional to $\sec(\theta)$ while the signal from D2 is proportional to $\sec(\theta+\phi)$ where ϕ is the inclination angle of D2. Assuming D1 and D2 are of the same thickness, for very high energy particles where the rate of energy loss does not vary significantly,

$$\frac{E_1}{E_2}=\frac{\cos(\theta+\phi)}{\cos(\theta)} \tag{1}$$

where E_1 and E_2 are the energy signals in D1 and D2, respectively. Thus, by inverting the equation, θ can be determined from the ratio of the signals. To extend the method to three dimensions, the third detector (D3) is inclined in the y-direction. The particle direction, both inclination and azimuth, can then be determined from the measured energy deposits with a pair of coupled equations. The actual ADIS equations, below, additionally take into consideration the changing energy loss rates.

In August 2004 we took a prototype ADIS charged particle instrument to the National Superconducting Cyclotron Laboratory (NSCL) at Michigan State University (MSU). Our tests at the NSCL had several goals: a proof-of-concept for the ADIS design; a calculation of the precision for the derived angle of incidence for charged particles, both in azimuth and declination; a determination of the ADIS response of our design as a function of the inclination of detectors; and a determination of the ADIS response of our design as a function of detector thickness.

As can be seen from Eq. (1), the determination of an energetic ion's angle of incidence, and hence the determination of its charge, depends on $\cos(\theta)/\cos(\phi+\theta)$, where ϕ is the angle of inclination of the ADIS detectors (D2 and D3) and θ is the incident particle's angle of incidence compared to the instrument normal direction. Clearly, since the above ratio gets farther from 1.0 as ϕ increases, a more accurate calculation of θ will result from larger values of ϕ. However, as ϕ increases, the effective geometrical factor of the telescope decreases (in fact, when ϕ reaches 90° the telescope has an effective geometrical factor of 0). Thus we expect an optimum range for the ADIS detector

inclination, ϕ, for a given application. Our NSCL tests were devised to address this issue.

One of the possible applications for a charged particle instrument in space is to measure Solar energetic particles. As these particles are more abundant at lower energy, the design of an instrument for this purpose would try to minimize the grammage of material (in this case silicon) necessary to make the calculation of the incident particle's angle of incidence (thus allowing for the measurement of particles at the lowest practical energies). However, when using silicon detectors in an ADIS system, the limitations on the detectors themselves will affect instrument design. As the thickness of silicon detectors decreases the signal to noise will decrease, making accurate charged particle determinations more difficult. Thus we would not expect to be able to use indefinitely thinner detectors to make this type of charged particle measurement. Again, our NSCL tests were developed to obtain direct data to study these issues.

While the original motivation for ADIS was elemental and isotopic resolution, the trajectory information ADIS provides can equally be used to study anisotropies and particle flows. Combined with magnetic field information, pitch angle distributions can be studied. As shown below, the ADIS prototype demonstrated an angular resolution of less than 4°.

2. Generalized theoretical ADIS response

In our earlier paper [2], we derived equations describing the response of an ADIS type instrument with D2 and D3 angled at 30° with respect to the horizontal, D2 with its normal vector in the x–z plane, and D3 with its normal in the y–z plane where z is the central axis of the instrument. Here we generalize with two inclined detectors at arbitrary orientation.

Consider an ADIS telescope (See Fig. 1). The normal unit vector, $\hat{n}_1$, to the plane of the top detector, D1, defines the central axis of the instrument along the z-axis, $\hat{k}$. Thus,

$$\hat{n}_1 = \hat{k} \tag{2}$$

The orientation of the first inclined detector, D2, is then defined by its normal unit vector

$$\hat{n}_2 = I_2\hat{i} + J_2\hat{j} + K_2\hat{k} \tag{3}$$

where

$$\begin{aligned} I_2 &= \sin\phi_2 \cos\varphi_2 \\ J_2 &= \sin\phi_2 \sin\varphi_2 \\ K_2 &= \cos\phi_2 \end{aligned} \tag{4}$$

ϕ_2 being the angle of inclination and φ_2 is the azimuthal angle. The definitions for D3 are similar.

A particle trajectory can be defined by the non-unit vector

$$\mathbf{p} = D_x\hat{i} + D_y\hat{j} + \hat{k} \tag{5}$$

with length equal to the secant of the angle of incidence between the particle and the instrument axis. The cosines of the particle trajectory with respect to each detector are then related via the dot products

$$\begin{aligned} \cos\theta_1 &= \frac{\mathbf{p}\cdot\hat{n}_1}{|\mathbf{p}|} = \frac{1}{\left(1 + D_x^2 + D_y^2\right)^{1/2}} \\ \cos\theta_2 &= \frac{\mathbf{p}\cdot\hat{n}_2}{|\mathbf{p}|} = \frac{I_2D_x + J_2D_y + K_2}{\left(1 + D_x^2 + D_y^2\right)^{1/2}} \\ \cos\theta_3 &= \frac{\mathbf{p}\cdot\hat{n}_3}{|\mathbf{p}|} = \frac{I_3D_x + J_3D_y + K_3}{\left(1 + D_x^2 + D_y^2\right)^{1/2}}. \end{aligned} \tag{6}$$

As before [2], we approximate the range of a heavy ion with a power law [3].

$$R = \kappa_0 \frac{A}{Z^2}\left(\frac{E}{A}\right)^{\alpha} \tag{7}$$

where A and Z are the mass and charge of the incident ion and κ_0 and α are empirically derived constants. Approximating $A = 2Z$ gives

$$R = \kappa \frac{E^{\alpha}}{Z^{\alpha+1}} \tag{8}$$

where κ incorporates the constant factor $2^{\alpha+1}$. For a particle stopping in D4, the range in D4 is then

$$R_0 = \kappa \frac{E_4^{\alpha}}{Z^{\alpha+1}} \tag{9}$$

where E_4 is the measured energy deposition in D4. Similarly,

$$\begin{aligned} R_0 + T_3\cos\theta_3 &= \frac{\kappa}{Z^{\alpha+1}}(E_4 + E_3)^{\alpha} \\ R_0 + T_3\cos\theta_3 + T_2\cos\theta_2 &= \frac{\kappa}{Z^{\alpha+1}}(E_4 + E_3 + E_2)^{\alpha} \\ R_0 + T_3\cos\theta_3 + T_2\cos\theta_2 + T_1\cos\theta_1 & \\ = \frac{\kappa}{Z^{\alpha+1}}(E_4 + E_3 + E_2 + E_1)^{\alpha} & \end{aligned} \tag{10}$$

where the T's are the detector thicknesses. Using the ADIS equations for the cosines of the angles gives four equations with four unknowns (Z, R_0, D_x and D_y). Solving simultaneously gives

$$\begin{aligned} D_x &= \frac{1}{I_2J_3 - I_3J_2}\left\{\frac{1}{T_1}\left[(E_4 + E_3 + E_2 + E_1)^{\alpha} - (E_4 + E_3 + E_2)^{\alpha}\right]\right. \\ &\quad \left.\times\left[\frac{J_3T_2}{(E_4 + E_3 + E_2)^{\alpha} - (E_4 + E_3)^{\alpha}} - \frac{J_2T_3}{(E_4 + E_3)^{\alpha} - E_4^{\alpha}}\right] - (J_3K_2 - J_2K_3)\right\} \\ D_y &= \frac{1}{I_3J_2 - I_2J_3}\left\{\frac{1}{T_1}\left[(E_4 + E_3 + E_2 + E_1)^{\alpha} - (E_4 + E_3 + E_2)^{\alpha}\right]\right. \\ &\quad \left.\times\left[\frac{I_3T_2}{(E_4 + E_3 + E_2)^{\alpha} - (E_4 + E_3)^{\alpha}} - \frac{I_2T_3}{(E_4 + E_3)^{\alpha} - E_4^{\alpha}}\right] - (I_3K_2 - I_2K_3)\right\} \\ Z &= \left[\frac{\kappa}{T_1}\frac{(E_4 + E_3 + E_2 + E_1)^{\alpha} - (E_4 + E_3 + E_2)^{\alpha}}{\left(1 + D_x^2 + D_y^2\right)^{1/2}}\right]^{1/(1+\alpha)}. \end{aligned} \tag{11}$$

For the special case of 30° angles of inclination, $\varphi_1 = 0°$ and $\varphi_2 = 90°$, these equations reduce, as they must, to those in our earlier paper [2].

It is worth noting that these equations require no trigonometric functions and can be solved using only logarithm and exponential functions which can be implemented in tables to minimize the processor requirements, facilitating on-board event processing.

3. Application of the ADIS equations

Besides their broader applicability to a range of ADIS configurations, the generalized ADIS equations are particularly useful in determining the precision required to construct a successful ADIS instrument, and in demonstrating that the physical parameters of an ADIS instrument can be derived from actual data to the precision required.

We begin with idealized Monte-Carlo data similar to that in our earlier paper [2]: D1, D2 and D3 have thicknesses of 50 μm; D2 and D3 are inclined at 30° to the instrument axis; the normal to D2 lies in the x–z plane, while that for D3 lies in the y–z plane. These data do not include instrument noise (a small effect for heavy ions) or Landau statistics (the dominant source of signal spreading for energetic heavy ions) and thus show clearly the effects of changes in angles or detector thickness on the analysis of data from an ADIS type instrument. As will be shown, the following nonetheless applies effectively to data that include both instrument noise and Landau statistics. In Fig. 2, Panels A and B show the Z determined using the ADIS technique for iron group elements Cr, Mn, Fe, Co and Ni with the correct instrument parameters. The curvatures in the elemental tracks in A are the result of the power-law approximation of the range (Eq. (7)). Additional scatter results from ions stopping or losing energy in detector rings or other support materials. In Fig. 2, Panels C and D show, respectively, the same data centered about Fe plotted against the D_x and the azimuthal angle of incidence (determined from D_x and D_y) for each event. Z is independent of both, and of D_y (not shown), as should be the case.

Fig. 3 Panels A and B show the result of assuming an incorrect D2 thickness of 51 μm in the analysis. As might be expected, this introduces a dependence on D_x in the Z determination, seen clearly in Panel A. There is no significant dependence on D_y (not shown). It also introduces a dependence on the azimuthal angle seen in Panel B. The effects of changing the D3 thickness are not shown, but are similar except that the effects are seen relative to D_y rather than D_x. Naturally, there is something of a degeneracy in that decreasing the D1 thickness is nearly equivalent to increasing the D2 and D3 thicknesses together. In other words, the method is most sensitive to the relative thicknesses, not the absolute thicknesses. The absolute thicknesses mainly impact the particle energy determination, not the charge and mass resolution, which is the primary goal of ADIS. Thus this is not a significant limitation, and applies generally to charged particle instruments where slight uncertainties in the detector

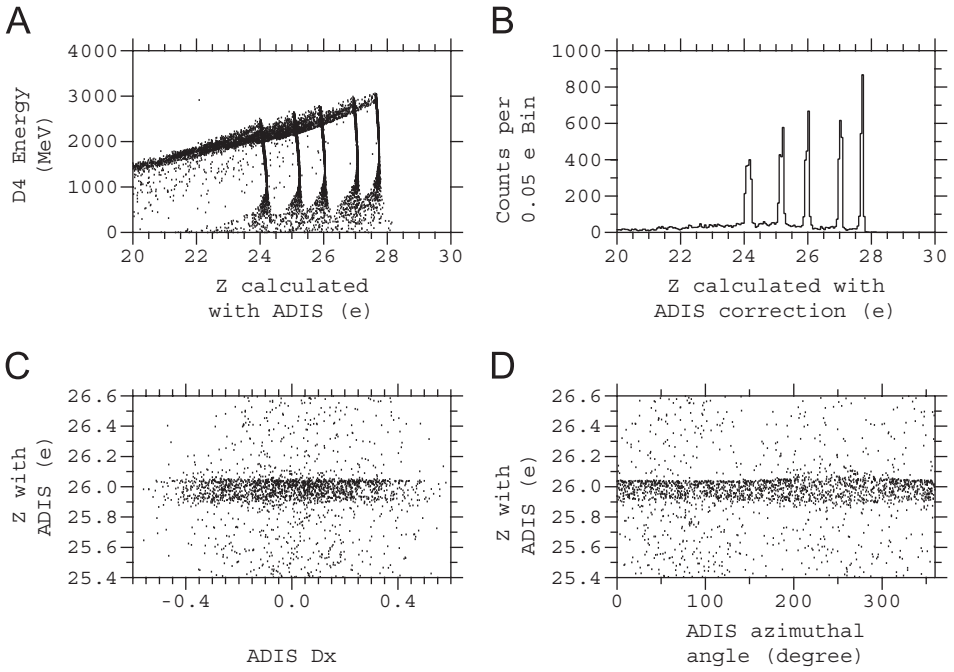

Fig. 2. Analysis of Monte-Carlo data showing the capabilities of the ADIS system on ideal iron-group data without noise. Panels A and B show the calculated elemental charge Z. Panel C shows the scatter of the calculated D_x near iron. Panel D shows the scatter of the calculated azimuth angle near iron. These panels show the data as calculated with the correct detector thicknesses, 50 μm, and correct orientations, D2 and D3 both inclined at 30° to the horizontal and rotated 90° with respect to each other.

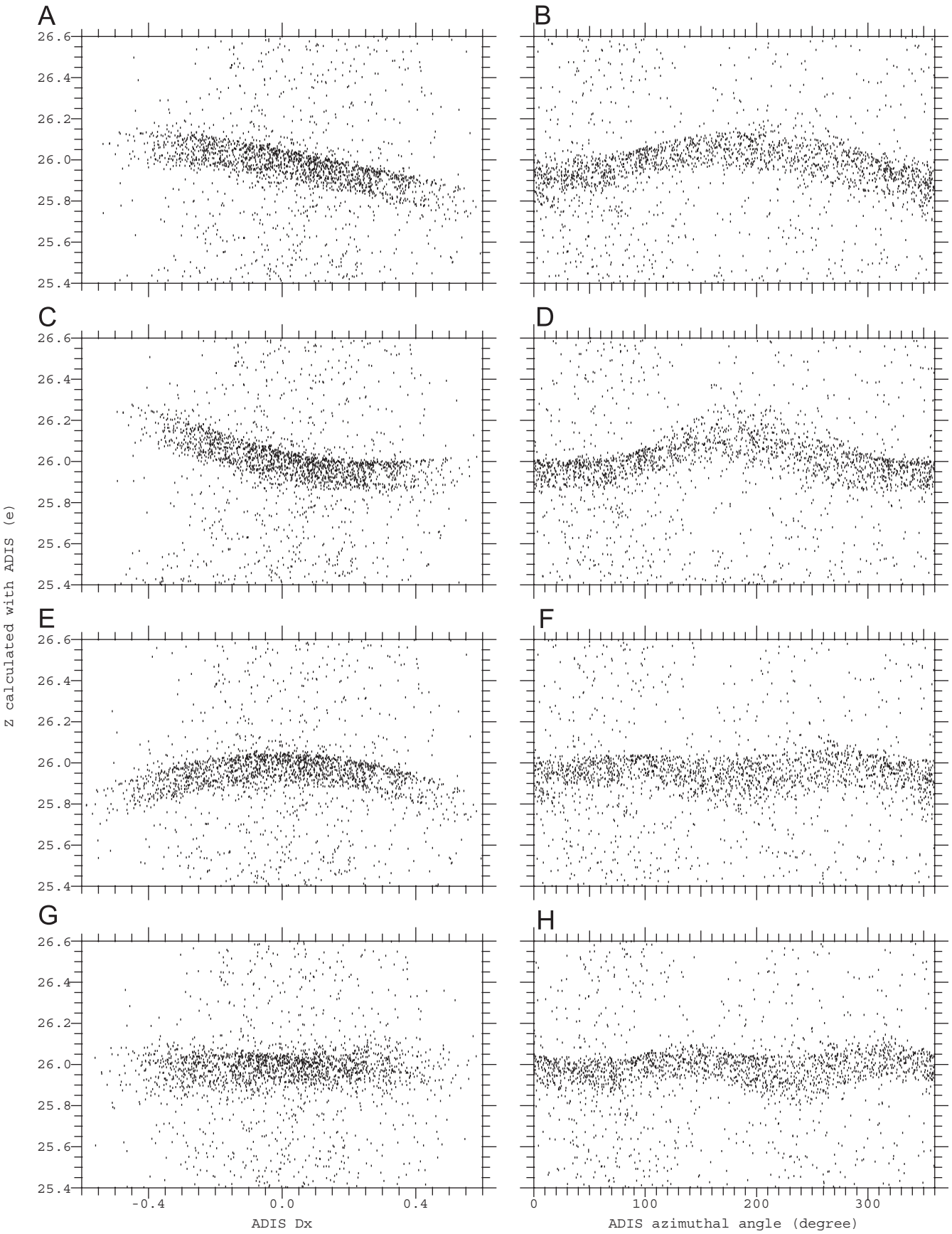

Fig. 3. These panels show the scatter of D_x and azimuth angle near iron for the same data as in Fig. 2; however, this is data that is analyzed using incorrect detector thicknesses and orientations. Panels A and B are calculated using incorrect thickness of 51 μm. Panels C and D are calculated using an incorrect inclination of 32°. Panels E and F are calculated using an incorrect thickness of 51 mm simultaneously with an incorrect inclination of 28°. Panels G and H are calculated using incorrect rotation of 95° (rather than 90°) between D2 and D3.

Table 1

	(a) Nominal	(b) Deduced	(c) Actual
D1 thickness (T_1)	50 μm	48 μm	48 μm
D2 thickness (T_2)	50 μm	49 μm	49 μm
D2 inclination (ϕ_2)	30°	29°	28°
D3 thickness (T_3)	50 μm	51 μm	51 μm
D3 inclination (ϕ_3)	30°	32°	32°
D3 rotation (φ_3)	90°	82°	80°

thicknesses result in slight systematic errors in the particle energy determinations. These must be corrected by other means.

Fig. 3 Panels C and D show the effects of changing the D2 angle of inclination from 30° to 32°. This too introduces dependencies on D_x and the azimuthal angle. To first order, changing the D2 angle of inclination is equivalent to changing the D2 detector thickness. In fact, as Fig. 3 Panel E shows, the effects are separable. In Fig. 3 Panels E and F, the D2 thickness has been increased to

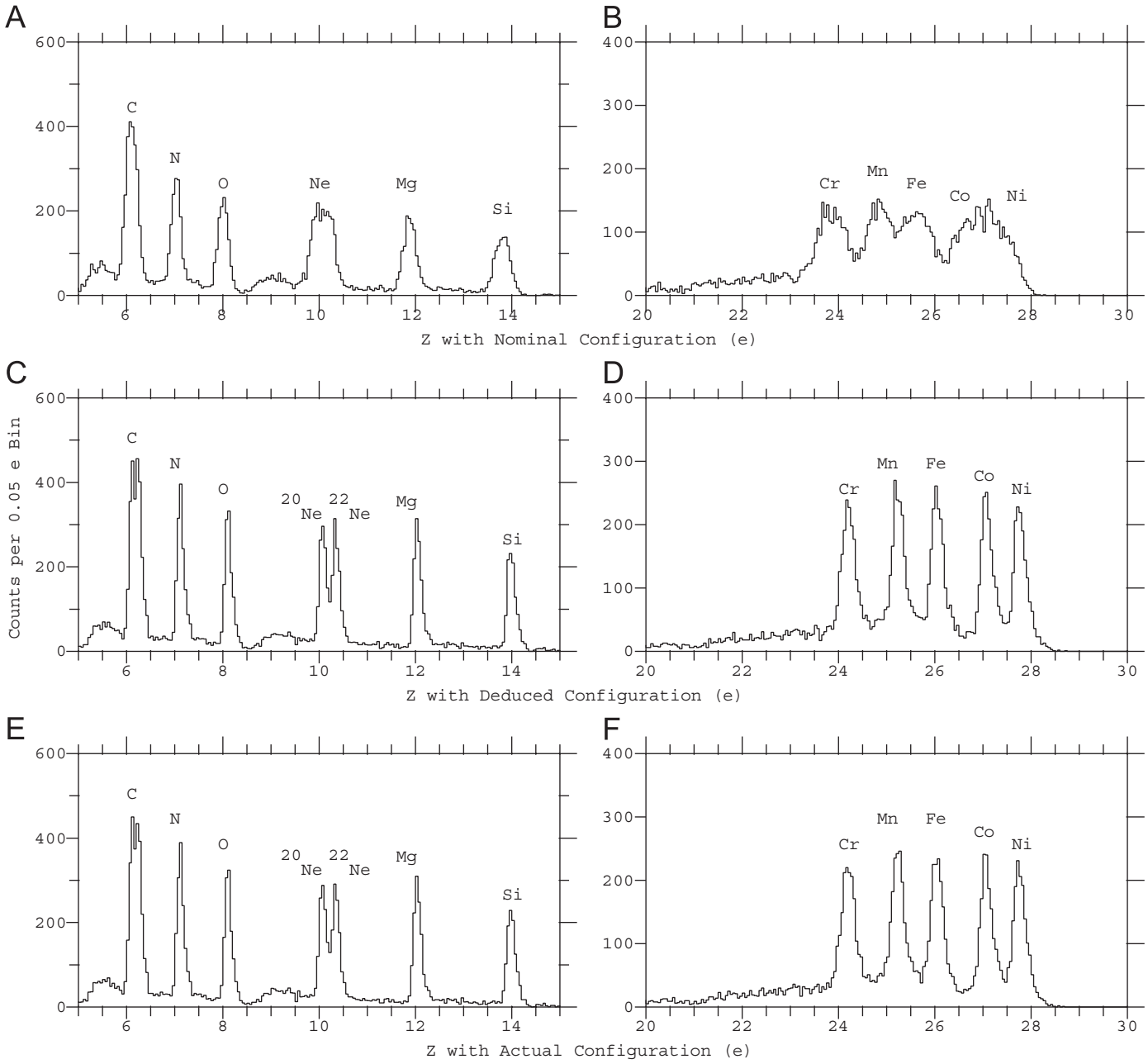

Fig. 4. Analysis of Monte-Carlo data that includes noise when the ADIS system orientation is not known a priori. Panels A and B show the calculated histograms of elemental charge when nominal, but incorrect assumptions are made about the ADIS system orientation. Panels C and D show the same histograms after using techniques to get best fits for the ADIS system orientation. Panels E and F show the same histograms using the known correct orientation.

51 μm and the D2 angle of inclination has been decreased to 28° in an attempt to compensate. While the linear dependence is removed, there remains a substantial curvature term. Thus, to determine the D2 thickness and angle of inclination relative to D1, a quadratic fit is made to Z as a function of D_x. The D2 thickness and inclination are then adjusted to reduce both the linear and quadratic coefficients. The same is done for D3 using D_y.

There remains the angle of rotation of the inclined detectors. Again, the absolute angles cannot be determined from the data, but the relative angle can be determined. Permitting D2 to define the x-axis, Fig. 3 Panels G and H show the results in the now familiar format for increasing the angle φ_3 to 95°. There is no dependence on D_x (nor D_y, not shown) but a clear dependence on the azimuthal angle, φ. In contrast to changing the detector thicknesses or angles of inclination, which can be well approximated by $A+B\cos(\varphi)+C\sin(\varphi)$, the data in Panel H is better fit by the form $A+B\cos(2\varphi)+\mathrm{C}\sin(2\varphi)$ and thus clearly distinguishable.

In order to verify that a correct ADIS configuration can be determined using ion data, one author (C.L.) generated Monte-Carlo data with thicknesses and angles differing slightly from the nominal values shown in column (a) of Table 1. These data included detector noise and an estimate of the Landau statistics. (As will be seen from the accelerator data, this estimate was slightly too conservative; the actual resolution we obtain during our accelerator run was slightly better.) The data were then analyzed by another author (J.J.C.), who was not told the actual values. The various thicknesses and orientations were iteratively adjusted in the manner indicated above to obtain the deduced values shown in Table 1 column (b). As can be seen from the actual values in column (c), the analysis came quite close to the correct values. Fig. 4 shows the utility of this approach. Panels A and B show the resolution obtained with the (erroneous) nominal values. Panels C and D show the much-improved results using the deduced values; the iron group elements are now clearly resolved as are the isotopes of neon. Panels E and F show the results using the actual values; these are nearly indistinguishable from the plots using the deduced values.

While, as noted above, only the thicknesses of D2 and D3 relative to D1 can be determined in isolation, if a determination of α and κ is made independently (as is the case here, using Monte-Carlo data produced for the nominal configuration) it is possible to determine the thicknesses of all three detectors from the data. This has significant implications if more than one instrument is to be built for comparison purposes in that it allows a close intercalibration. Such multi-spacecraft space missions are by no means rare: CLUSTER, the upcoming STEREO and MMS and the proposed Solar Sentinel missions are examples.

From this blind test, it is clear that the actual configuration of an ADIS type instrument can be determined using ion data with sufficient precision as to

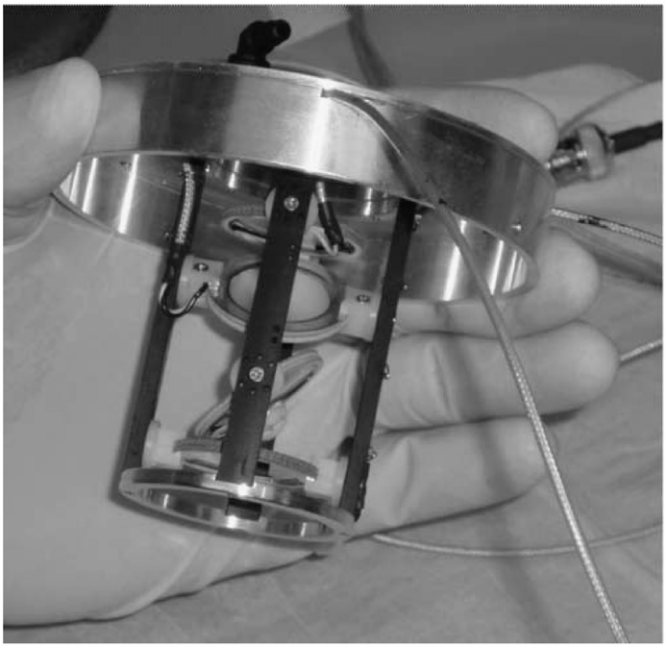

Fig. 5. Prototype ADIS charged particle telescope taken to NSCL for beam testing. Note the pivoting mounts for the ADIS detectors D2 and D3.

Table 2
Best fit constants of the elemental charge determination

ADIS detector thickness (μm)	α	κ
200	1.60±0.01	15.2±0.2
100	1.67±0.01	13.0±0.2
50	1.65±0.01	14.0±0.2

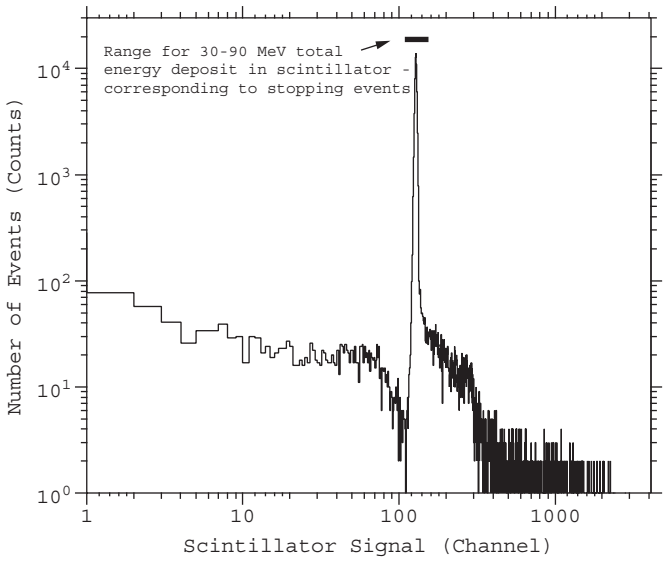

Fig. 6. Scintillator response. A large proportion of valid D4 stopping events included a signal in the PMT channel, with ~85.2% of D4 stopping particles having a coincident signal in the scintillator. This signal was generally in the range of 30–90 MeV total energy, as marked by the solid bar.

obtain effectively full resolution from the instrument. These ion data could be obtained in flight, or during an accelerator calibration. It should also be noted that the angular precision required in mounting the detectors is extraordinarily modest, $\sim 1^{\circ}$.

4. Test instrument design and accelerator exposure

Fig. 5 is a picture of the instrument we took to the NSCL; Fig. 1 is a schematic of the instrument design. The D1, D2 and D3 detectors are termed the ADIS detectors. The D4 detector is the stopping detector and is 1000 μm thick. These four detectors are fully depleted silicon surface barrier detectors. The D2 and D3 detectors (Fig. 5) are held with pivoting mounts. The mounts can be moved to set the D2 and D3 detectors at inclinations of 15°, 30° and 45° to the telescope normal axis. The ability to re-orient these detectors allowed us to perform the desired studies. In this first test of the ADIS system, all four detectors were circular detectors—in future instruments D2 and D3 will be oval with a planar projection identical to the aperture defined by the circular D1 and D4 detectors. For practical purposes, D2 and D3 detectors were circular: since the eccentricity of the ovals depends upon the angle of inclination, the use of oval detectors for our prototype testing would have required not merely three sets of D2–3 detectors (for 50, 100 and 200 μm) but different shapes for each inclination for a total of nine sets. It would also have required complete disassembly of the instrument each time we changed detector inclination.

Surrounding these four detectors is a plastic scintillator, painted on the interior surface with $BaSO_4$ reflective white paint. This entire assembly is surrounded with a reflective light box viewed by a photomultiplier tube. All the signals were read out through NIM bin pre-amplifiers, shaping amplifiers and coincidence modules to a VME system with a peak detect sample and hold card, and the signals were stored in raw channel number (0–4095). In order to easily manipulate the detectors, the telescope stack was a removable fixture in the light box. We came to the NSCL with two different ADIS telescope stacks; thus, detectors could be changed in one stack while the other was in the beam.

The test design was developed for the greatest flexibility in testing (as addressed above) with the minimum necessity for direct physical manipulation of the fragile silicon detectors. This necessarily compromised the design: for example, the structure supporting the detectors was complex so the detectors could be rotated and this added undesirable dead material to the instrument (see Fig. 5). It was also rather robust to permit rapidly changes of detectors during the run.

The instrument was designed to permit rapid changes of Si telescope stacks in the scintillator cup. Also, since we

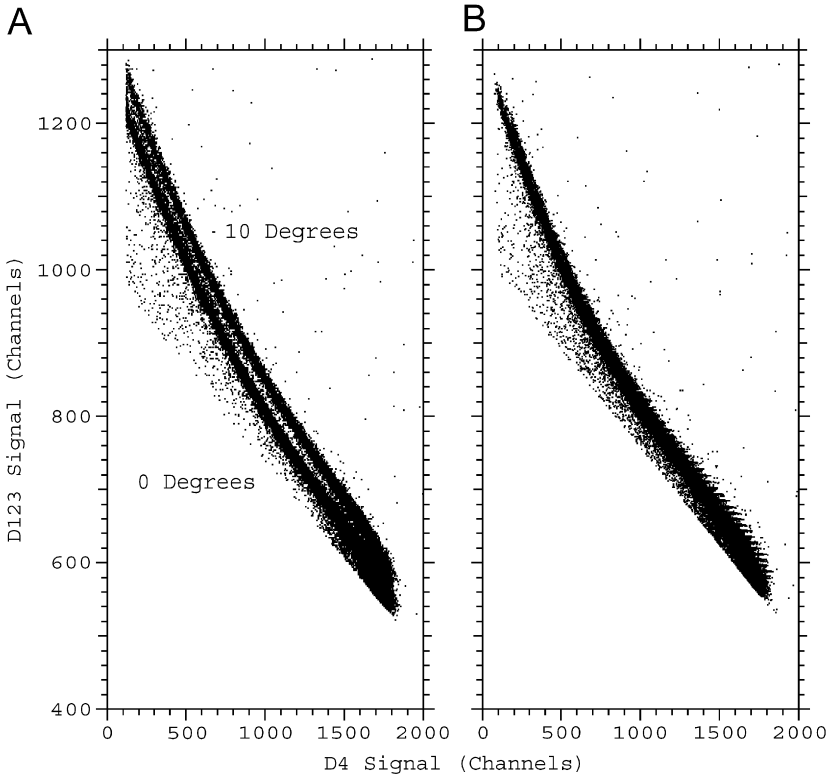

Fig. 7. Scatter plots of the sum of the energy deposit in D1 + D2 + D3 versus the residual energy in D4. This data is for 200 μm thick ADIS detectors with D2 and D3 inclined by 30° placed in a primary beam of ^{48}Ca. Two beam runs, one with the instrument aligned with the beam and the other with the instrument rotated by 10° to the beam axis are shown. Panel A shows the raw uncorrected data and Panel B shows the data after correcting for the incoming particles' angles of incidence.

used circular detectors for D2 and D3, their ring mounts were to some extent directly in the telescope aperture, and added inert material in which incident particles could deposit energy, also increasing our background. In a flight instrument, these problems would be addressed using appropriate designs.

The CCF supplied us with a primary beam of ^{48}Ca. Ca, with a nuclear charge of 20, is sufficiently close to the nuclear charge of Ni (28) that the results of these analyses are a good indicator of how an ADIS charged particle instrument will function in space, where $>99.9\%$ of all particles have nuclear charge $\leqslant 28$. In addition to the primary beam, we also were supplied with a fragment beam from the ^{48}Ca source. This fragment beam contained measurable amounts of the five sub-Ca elements, P, S, Cl, Ar and K, giving us a mix of ions for more realistic simulation of measurements in space. In the rest of this discussion we refer to these possible beams as "primary" runs and "fragment" runs. We had 18 h of beam time; each run lasted approximately 5 min, and, as the beam strength varied from run to run, we collected on the order of several hundred thousand to a million events during each run. In order to effectively simulate omni-directional space radiation, our instruments were mounted on a moveable turntable. We rotated the turntable from -20° to $+20^\circ$, in 5° increments, across the nominal beam axis, thus simulating an isotropic flux in one angular dimension. In order to simulate an isotropic flux in the other angular direction we manually rotated the instrument on its platform.

An energy degrader, in the form of a wedge of aluminum, 2.0 mm thick at the top tapering to 0.1 mm thick at the bottom was constructed. This wedge was continuously raised and lowered into the beam in front of our instrument aperture using a motor. Thus the nearly monoenergetic CCF beams were spread in energy to simulate space radiation. While we knew how each of these effects was achieved, the final analyses of the incident charged particles were done "in the blind" thus giving us a reasonable simulation of the true space environment.

5. Data analysis

To determine an incoming ion's elemental charge, we need to determine the empirical coefficients α and κ, as shown in Eq. (8). We determined the values of α and κ using data from the primary runs. This was done because in the case of the primary beam runs the total number of counts in the single Ca peak was greater (by a factor $\sim$6) than the total number of counts in the six element peaks in fragment runs. Since α and κ are weak functions of energy (See Fig. 2) this was done for the three D1–D3 detector thicknesses, combining data from the various D2–D3 inclinations in each fit. Thus we have three sets of α and

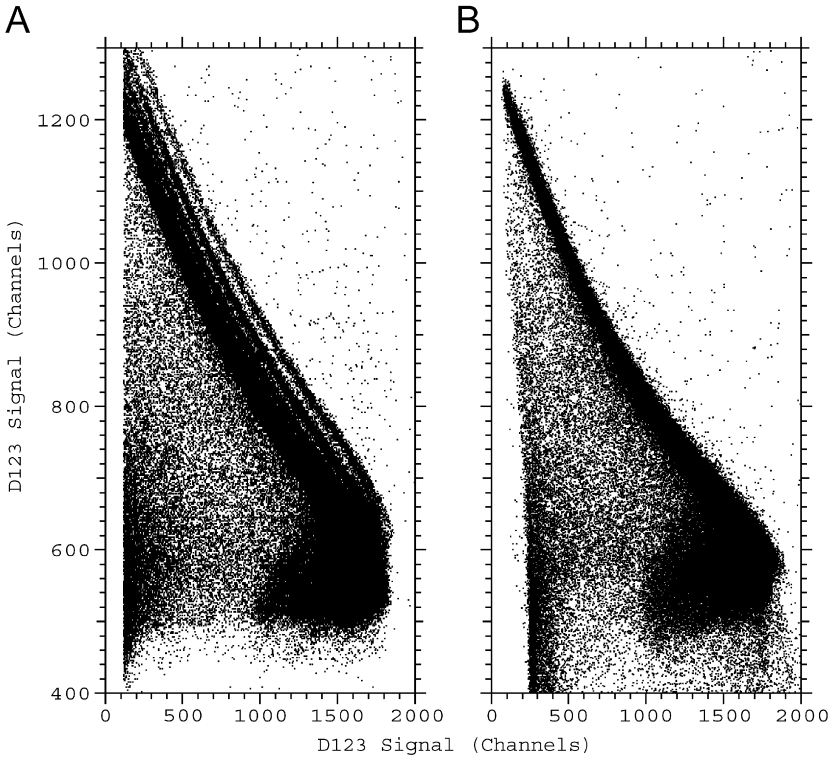

Fig. 8. Scatter plots of the sum of the energy deposit in D1 + D2 + D3 versus the residual energy in D4. This data is for 200 μm thick ADIS detectors with D2 and D3 inclined by 30° placed in a primary beam of ^{48}Ca. We show nine beam runs with the instrument axis rotated by -20°, -15°, -10°, -5°, 0°, $+5^\circ$, $+10^\circ$, $+15^\circ$ and $+20^\circ$ with respect to the nominal beam axis. Panel A shows the raw uncorrected data and Panel B shows the data after correcting for the incoming particles' angles of incidence using ADIS. After the angle correction tracks for all nine different angles of incidence are aligned in a single Ca track.

κ for our data, corresponding to the 200 μm thick detectors, the 100 μm thick detectors and the 50 μm thick detectors. All runs using a particular thickness of detectors, whether primary or secondary, and regardless of the angle of inclination of the D2 and D3 detectors, are analyzed using the same α and κ. This analysis method is exactly how we would analyze data from a functioning instrument in space. The values of α and κ used in all the analyses are listed in Table 2.

The calculation of the elemental charge described above assumes that the particles in question stop in the D4 detector. The beam energy for the ^{48}Ca was degraded to ~80 MeV/nucleon, which for some angles of incidence and ADIS detector inclinations passes completely through the detector stack, at which point these ions would trigger the plastic anti-coincidence cup surrounding the telescope stack. The original intention was to simply use signals in the anti-coincidence cup to exclude particles that did not stop in D4 from the full analysis. However, a large proportion of valid D4 stopping events included a signal in the PMT channel. It is possible this resulted from a light-leak, or electronic cross talk. Most of the incident particles (85.2%) had associated signals in the scintillator channel of between 30–90 MeV total energy (Fig. 6), corresponding to ~0.6–1.9 MeV/nucleon of ^{48}Ca. When a particle with a scintillator energy deposit anywhere in the range 30–90 MeV total energy also had a ratio of energy deposits Scintillator/D4 of less than 2% we considered that particle to have stopped in D4. This technique is the selection criterion applied to all runs to determine whether particles stopped in D4 or whether they penetrated the entire stack.

For an actual flight instrument, we would anticipate having a separate solid state detector at the bottom of the stack to identify penetrating particles within the instrument

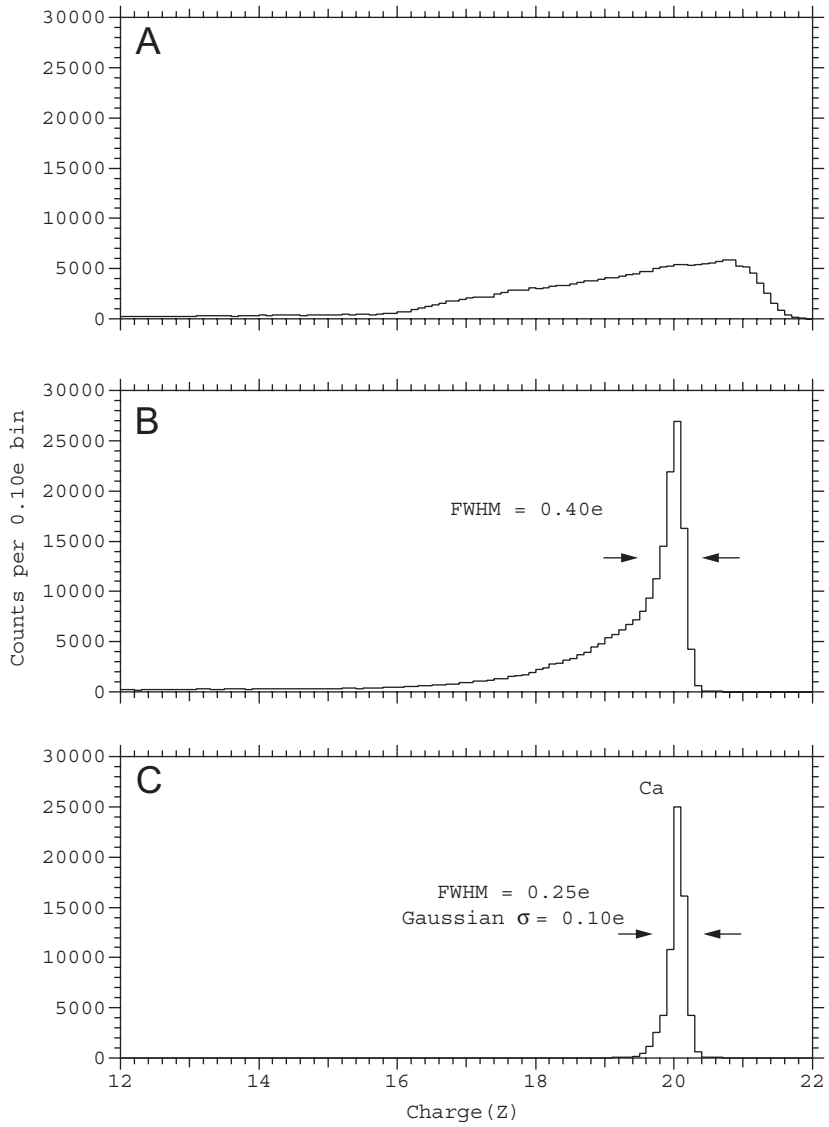

Fig. 9. Elemental charge histograms for the data shown in Fig. 8. Panels A and B correspond directly to Fig. 8 A and B. Panel C shows the charge histogram after selection for only particles stopping in D4.

viewing cone, while scintillator would be used to identify side-penetrating events. The scintillator cup was used here for simplicity.

In Fig. 7 we show a scatter plot of the sum of the energy of particles deposited in D1 + D2 + D3 versus the residual energy deposited in D4 for particles from two primary runs of ^{48}Ca. In these runs the ADIS detectors are 200 μm thick and are inclined at an angle 30°. The two runs are with the instrument normal axis aligned with the beam and with the instrument normal axis rotated by 10° with respect to the beam. Panel A shows how the uncorrected data from these two runs compare, with the 10° offset run lying well above the 0° run. Once we make the correction for angle of incidence, as determined with the ADIS system, the scatter plots for these two runs overlie each other (Panel B). In Fig. 8 we show the same type of scatter plot, but this time with ALL the data from this primary run, with the instrument normal axis oriented at −20°, −15°, −10°, −5°, 0°, +5°, +10°, +15° and +20° to the beam. Again Panel A shows the uncorrected data and Panel B shows the ADIS corrected data. The backtracks (in the lower right hand corner) are from particles which penetrate the entire telescope stack and do not stop in D4. In Fig. 9 we show a histogram of the derived charge for the complete set of 9 runs listed above—200 μm thick detectors inclined at 30°. Panel A shows the histogram of calculated elemental charge with no angle corrections, Panel B is a histogram of the calculated charge after the ADIS correction has been made, and Panel C is the histogram after we make the selection for only particles which stop in D4 (as described above). It is clear that the ADIS correction for angle allows for excellent particle identification—the sigma to a Gaussian fit of the fully corrected stopping particles is 0.10*e* (charge units) when looking at a single element.

In Fig. 10 we show scatter plots for a series of fragment runs. The detector thicknesses in this scatter plot are 200 μm and the ADIS detectors are inclined at an angle of 30°. Again, this is a compilation of nine runs, with the instrument normal axis oriented at −20°, −15°, −10°, −5°, 0°, +5°, +10°, +15° and +20° to the beam. Panel A shows the uncorrected data and Panel B shows the ADIS corrected data. Again we see that the ADIS angle correction properly collapses the data into tracks for each individual element. Fig. 11 shows the histograms obtained from the calculation for the charge with all nine runs combined. Panel A (corresponding to the scatter-plot Panel A) shows the charge histogram obtained when no correction for angle of incidence is made. Here, while there appear to be peaks in the distribution, they are not aligned on unit charges, and are merely an artifact of the data where, for example, a +20° beam angle has the P track falling on top of the track for Cl at +5°—but the derived charge with no angle calculation for each is incorrect. In Panel B (corresponding to the scatter plot Panel B) we show the charge histogram obtained after the ADIS angle correction is applied to all nine of these runs. Now six

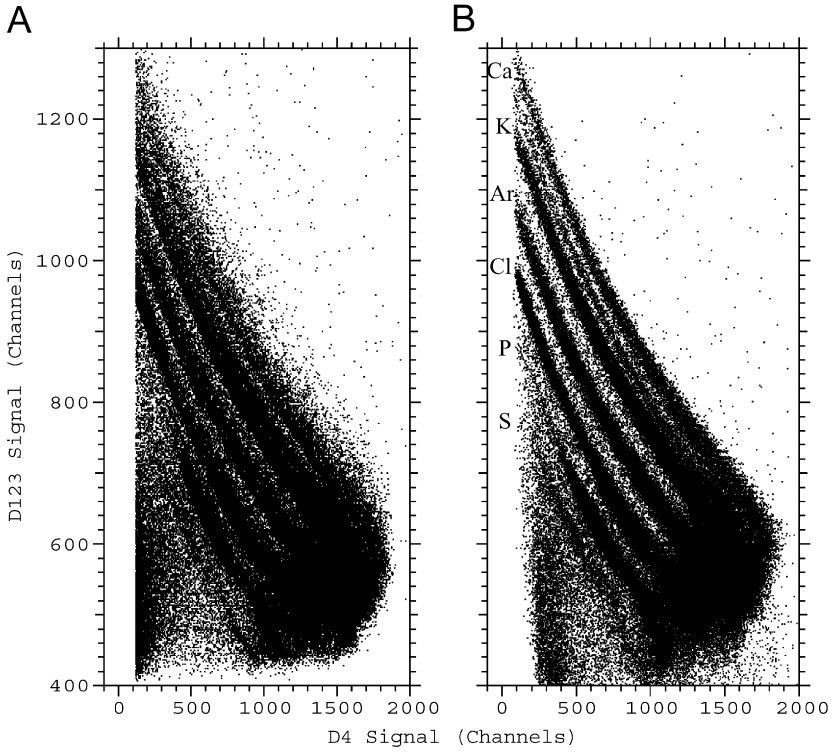

Fig. 10. Scatter plots of the sum of the energy deposit in D1 + D2 + D3 versus the residual energy in D4. This data is for 200 μm thick ADIS detectors with D2 and D3 inclined by 30° placed in a fragment beam from a ^{48}Ca source. We show nine beam runs with the instrument axis rotated by −20°, −15°, −10°, −5°, 0°, +5°, +10°, +15° and +20° with respect to the nominal beam axis. Panel A shows the raw uncorrected data and Panel B shows the data after correcting for the incoming particles' angles of incidence using ADIS. After the angle correction tracks for six different elements are separated.

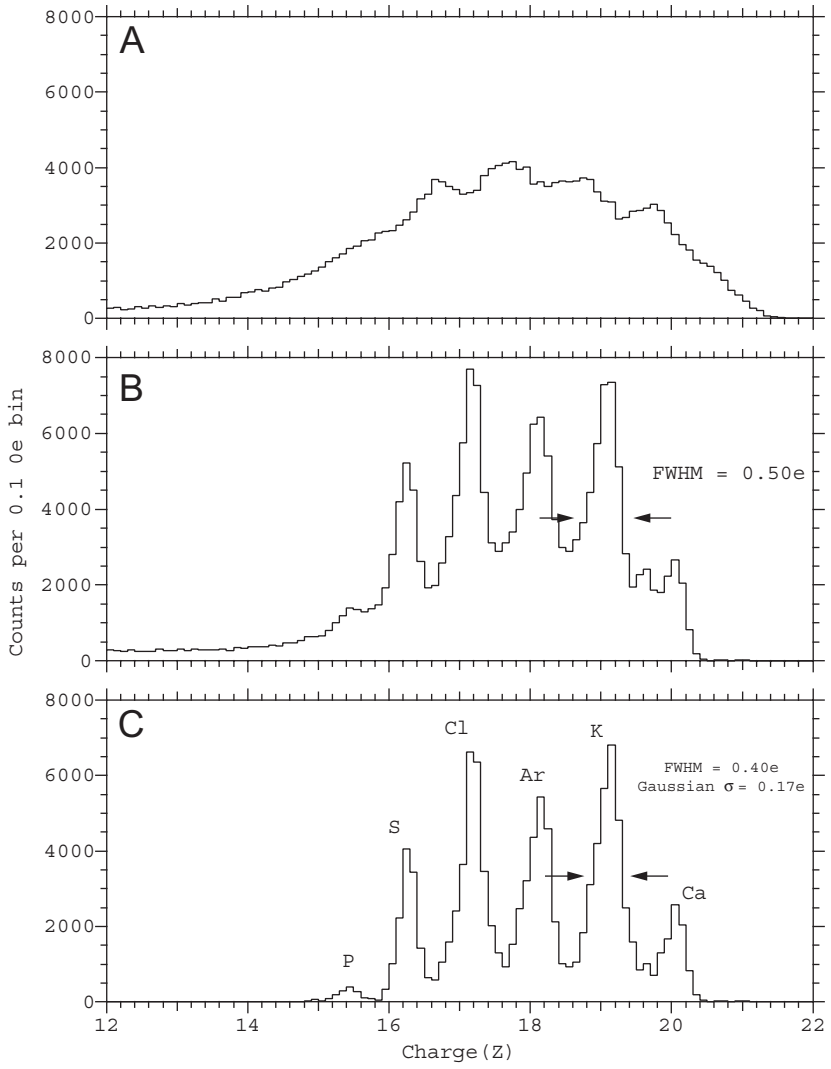

Fig. 11. Elemental charge histograms for the data shown in Fig. 10. Panels A and B correspond directly to Fig. 10 A and B. Panel C shows the charge histogram after selection for only particles stopping in D4. After selection for stopping particles peaks for all six elements are cleanly resolved and background has been reduced to $\leqslant 20\%$ of peak counts.

peaks are distinguished, and each lies on a unit charge corresponding to the elements from P to Ca. Panel C shows the charge histogram obtained when a selection for stopping particles is made. Again we see how the ADIS correction gives reasonable particle identification; here the best-fit Gaussian sigma, for the widest peak, is 0.17*e*.

Fig. 12 shows the charge histograms for all of the fragment runs, with the data from all of the beam orientations with a given set of detectors at a given ADIS detector inclination compiled into a single histogram. That is, the 50 μm at 15° histogram (Panel A) contained all the data from five runs, −20°, −10°, 0°, +10° and +20° each taken with 50 μm thick ADIS detectors with D2 and D3 inclined at 15° compared to D1. Table 3 lists the sigmas for the widest of the best-fit Gaussians to each of the histograms. Table 4 lists the sigmas for the best-fit Gaussians to the primary beam of ^{48}Ca—these are generally smaller values than for the fragment beam because there is only one element, Ca, in the primary runs while the secondary runs have overlapping peaks for six elements. We did not have time to complete the runs using 50 μm detectors inclined at 45°.

Reading across each of the rows in Tables 3 and 4 allows us to determine how the angle correction varies as a function of angle of inclination of the ADIS detectors. In all cases the 30° fits are better than the 15° fits, and generally the 45° fits are better than the 15° fits though slightly worse than the 30° fits. The behavior of the ADIS system as a function of inclination of the ADIS detectors follows the pattern we had originally hypothesized—that a range of intermediate angles would give the best possible charge discrimination. We believe that an ADIS inclination of 30–45° is the most likely to give optimum charged particle discrimination.

Reading down each column in Tables 3 and 4 we can see how the ADIS system varies as a function of the thickness of the ADIS detectors. Here we see that the 50 μm detectors are always giving poorer elemental charge

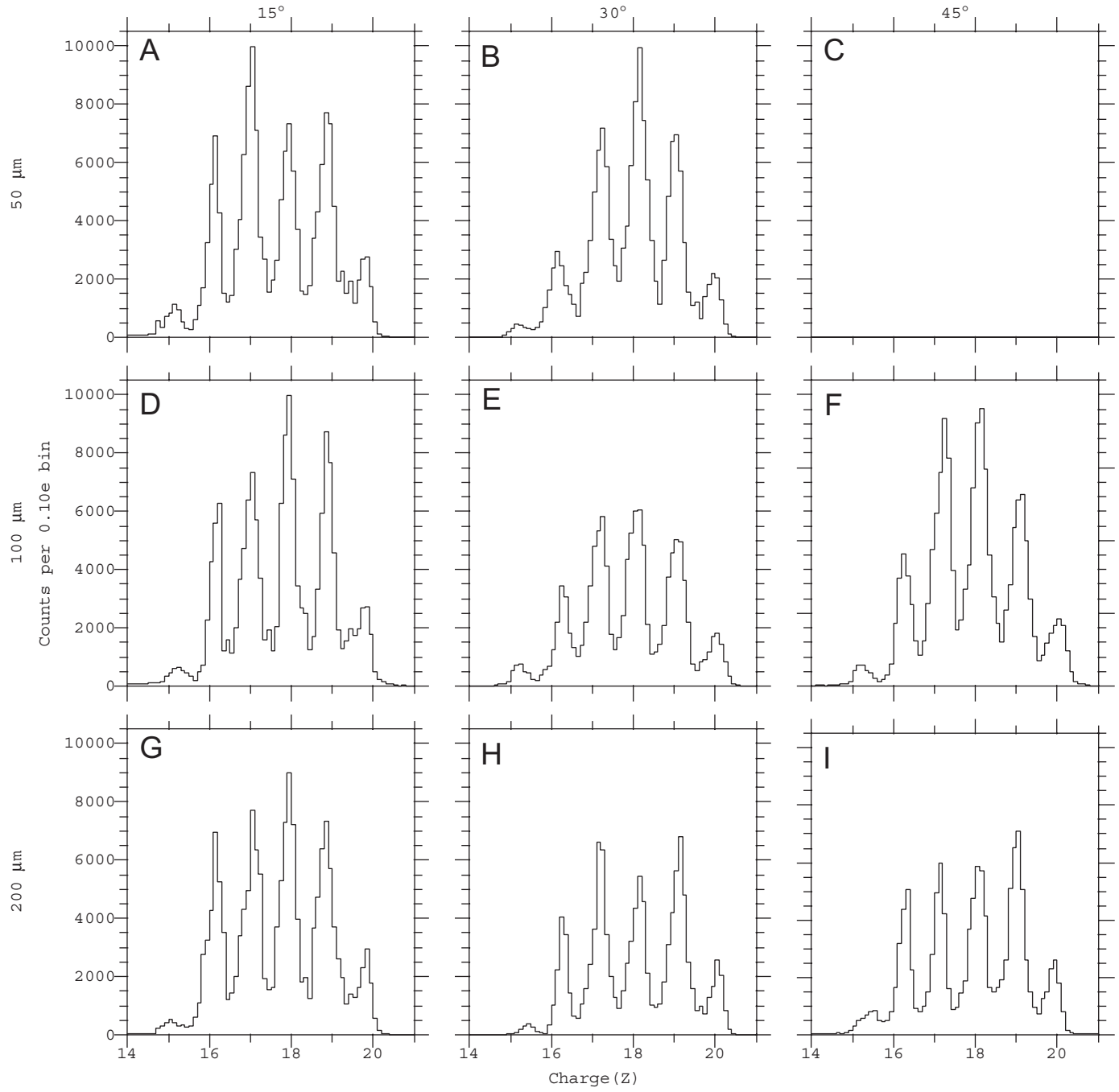

Fig. 12. Histograms of the calculated elemental charge for the nine possible configurations of our ADIS detectors. All panels show data of fragment runs from a ^{48}Ca source. Each panel has all the data for every rotation of the instrument with respect to the nominal beam axis: $-20°$, $-15°$, $-10°$, $-5°$, $0°$, $+5°$, $+10°$, $+15°$ and $+20°$. For detector thicknesses: Panels A, B and C are using 50 μm detectors; Panels D, E and F are using 100 μm detectors; Panels G, H and I are using 200 μm detectors. For ADIS detector inclinations: Panels A, D and G are using 15° inclination; Panels B, E and H are using 30° inclinations; Panels C, F and I are using 45° inclinations. (There is no data for the 50 μm thick detectors inclined at 45°—Panel C).

Table 3
Sigma of best-fit Gaussians to charge histograms for secondary ^{48}Ca beams

	15°	30°	45°
50 μm	0.19±0.023	0.17±0.015	No data taken
100 μm	0.14±0.012	0.16±0.016	0.20±0.024
200 μm	0.18±0.012	0.17±0.017	0.17±0.020

Table 4
Sigma of best-fit Gaussian to charge histogram for primary ^{48}Ca beams

	15°	30°	45°
50 μm	0.21±0.062	0.15±0.026	No data taken
100 μm	0.17±0.024	0.12±0.020	0.16±0.030
200 μm	0.13±0.020	0.10±0.022	0.10±0.035

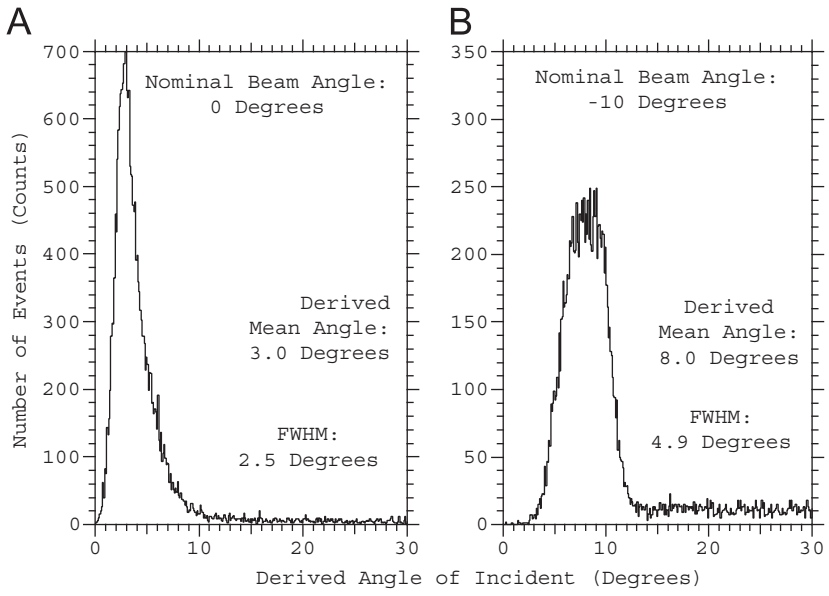

Fig. 13. Derived angles of incidence for primary (^{48}Ca) beam runs with the instrument aligned at 0° and rotated by −10° to the nominal beam axis. The offset of 2–3° is most likely due to a misalignment of our instrument when we manually mounted it on the turntable supplied by the NSCL. These runs are for ADIS detectors of 200 μm thickness inclined at 45° to the instrument axis.

discrimination. The 200 μm detectors and 100 μm detectors are about equal in their ability at elemental charge discrimination, with perhaps a slight improvement in the 200 μm detectors as compared to the 100 μm detectors. The ADIS system's performance with respect to thickness of the ADIS detectors also follows our original ideas—thicker detectors will give more accurate results.

The ADIS system will calculate, as a matter of necessity, the angle of incidence of incoming particles. In Fig. 13, we show histograms for the derived angle of incidence of charged particles for two runs, with 200 μm ADIS detectors inclined at 45°. The two runs are for our instrument aligned along (Panel A) and oriented at 10° (Panel B) to a primary ^{48}Ca beam. As can be seen in these panels, the ability to accurately determine a particle's angle of incidence decreases as the particles enter farther off-axis. However, even in the worst cases, the angular distributions have a full-width at half-max of ~8° (corresponding to a Gaussian sigma of ~3.5°).

We also noted that in all of our 137 beam runs, the mean of the derived particle angle of incidence differed from the nominal assumed angle by 2–3° (Fig. 13 shows two examples). The most likely explanation is that the turntable upon which we placed our instrument had its 0° axis misaligned with the beam axis by about 2–3°. This misalignment could easily have occurred because we manually adjusted the NSCL apparatus so that the beam would pass through the center of our instrument, not the center of their turntable, and since we did not require extremely accurate angular alignment this manual adjustment was checked only by eye.

6. Conclusions

We have extended and generalized the ADIS equations. Applying those equations to Monte-Carlo data we have determined that the precision requirements on the detector orientations and thickness to achieve good charge resolution in the iron region are modest. Furthermore, we have demonstrated that the thicknesses and orientations can be deduced from heavy ion data, either in flight or from accelerator calibrations, to the precision needed.

We have tested ADIS models using ^{48}Ca primary and fragment beams. Despite the design compromises in these models, the results were very encouraging. Elements were clearly resolved with a resolution of $<0.25e$, thus validating our earlier Monte-Carlo simulations. We can easily determine an incident particle's angle of incidence to 5° or better. Nonetheless, the background remains significant, particularly as in-flight the odd number elements are much reduced in abundance compared to even number elements. The primary source of the background events is ions passing through or stopping in dead material, one particular source being the rings on the circular—as opposed to oval—inclined detectors.

Our next objective is to further develop and test a more advanced ADIS prototype in a near-flight configuration to demonstrate the full capabilities of an ADIS instrument. The most critical improvement in the new prototype will be the oval D2–3 detectors at a fixed angle of 30° of inclination, as suggested by the above work. It will have a minimum of dead material inside the scintillator, resulting in a much reduced level of background. We are studying the possibility of extending scintillator into the

space between detectors to partially shield the detector rings and support structure. As in our previous beam run, the instrument will be tested at varying angles to simulate the isotropic space radiation, and we will provide a degrader to vary the energy as would be seen in space.

The results of this run will provide a compelling demonstration of the capabilities to be expected in an actual ADIS flight instrument. Despite the substantial amount of dead material in the test instrument, the accelerator data shows exceptional charge resolution for so simple an instrument. An instrument providing data of this quality is attractive for many space applications even without the improvements in background to be expected in future instruments. This is of particular importance in both raising the Technical Readiness Level and mitigating risk for ADIS-based instruments for future flight opportunities.

Acknowledgments

We would like to thank the staff of National Superconducting Cyclotron Laboratory for their support and assistance with our beam exposure. Particular thanks are due to Dr. Raman Anantaraman for general support and to Dr. Ron Fox for assistance with the VME data acquisition system and software.

Thanks are also due to Jeff Nault for work on the data acquisition system.

The ADIS instrument development project was 95% funded by NASA under the Living With a Star (LWS) Targeted Research and Technology program (Grant NAG5-12493).

References

[1] J.A. Simpson, in: Annual Review of Nuclear and Particle Science, Vol. 33, Annual Rev. Inc., Palto Alto, CA, 1983, 323pp.
[2] J.J. Connell, C. Lopate, R.B. McKibben, Nucl. Instr. and Meth. 457 (2001) 220.
[3] Koon H. Lau, CalTech Ph.D. Thesis, 1985.